Thermodynamic Analysis of Self-Assembly in Coiled-Coil Biomaterials

ARTICLE *in* BIOCHEMISTRY · SEPTEMBER 2011

Impact Factor: 3.02 · DOI: 10.1021/bi201038j · Source: PubMed

5 AUTHORS, INCLUDING:

Bashkim Kokona
Haverford College
26 PUBLICATIONS **316** CITATIONS
SEE PROFILE

Robert S. Manning
Haverford College
22 PUBLICATIONS **344** CITATIONS
SEE PROFILE

Robert Fairman
Haverford College
78 PUBLICATIONS **3,745** CITATIONS
SEE PROFILE

BIOCHEMISTRY
including biophysical chemistry & molecular biology

Article

pubs.acs.org/biochemistry

Thermodynamic Analysis of Self-Assembly in Coiled-Coil Biomaterials

Betty P. Tsang,[†] Heidi S. Bretscher,[†] Bashkim Kokona,[†] Robert S. Manning,[‡] and Robert Fairman*[,†]

[†]Department of Biology and [‡]Department of Mathematics, Haverford College, 370 Lancaster Ave., Haverford, Pennsylvania 19041, United States

Supporting Information

ABSTRACT: Coiled-coil protein structural motifs have proven amenable to the design of structurally well-defined biomaterials. Mesoscale structural properties can be fairly well predicted based on rules governing the chemical interactions between the helices that define this structural motif. We explore the role of the hydrophobic core residues on the self-assembly of a coiled-coil polymer through a mutational analysis coupled with a salting-out procedure. Because the resultant polymers remain in solution, a thermodynamic approach is applied to characterize the polymer assembly using conventional equations from polymer theory to extract nucleation and elongation parameters. The stabilities and lengths of the polymers are measured using circular dichroism spectropolarimetry, sizing methods including dynamic light scattering and analytical ultracentrifugation, and atomic force microscopy to assess mesoscale morphology. Upon mutating isoleucines at two core positions to serines, we find that polymer stability is decreased while the degree of polymerization is about the same. Differences in results from circular dichroism and dynamic light scattering experiments suggest the presence of a stable intermediate state, and a scheme is proposed for how this intermediate might relate to the monomer and polymer states.

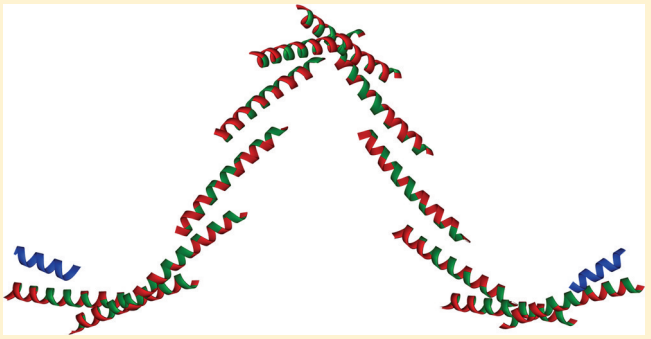

The successful engineering of biomaterials has led to important advances in a wide array of applications, including tissue engineering,[1] biomineralization,[2] and photoelectronics.[3−5] While a range of biomolecules have been exploited for such engineering, arguably the incorporation of proteins and peptides into biomaterials has the greatest promise because of a variety of favorable properties. Such properties include biocompatible and biodegradable characteristics, reversible responsiveness to their environment, and the ability for scientists to design mesoscale structures derived from well-understood atomic-level interactions.[4,6−8]

While many different types of protein structural motifs have been exploited, the rich history of work on the coiled coil, a motif involving precisely understood helix pairing interactions, makes it particularly amenable to the design of biomaterials. Many reviews have been written on the use of this motif in design and bioengineering work, and only a few recent reviews are cited here.[9−11] Most relevant to the work described herein, both the Woolfson laboratory and the Conticello laboratory have described the successful engineering of a wide variety of mesoscale structures using the coiled coil.[10,12−22]

Our own work in this area has taken advantage of the coiled coil from the well-studied yeast transcription factor, GCN4.[23−26] We described the development of a biomaterial using this structural motif a number of years ago.[27] Briefly, we had designed a 30-residue peptide containing tandem 14-residue sequences from the GCN4 coiled coil, separated by a two-alanine spacer sequence. The 14 residues of each individual repeat, when folded into a helical conformation, form an amphipathic structure. The consequence of the two-alanine spacer is to create a structure with two hydrophobic faces that are phased at ∼200° with respect to one another. Such a structure is therefore incapable of forming a dimer with a continuous hydrophobic interaction at its interface (Figure 1; the sequence of the peptide used in this earlier study, CpA, is shown as well). Thus, if the peptide can be induced to form a coiled-coil interaction, it would result in an offset interaction in which the resultant high-energy nucleus could presumably act as a template for bidirectional growth. We had characterized the resultant biomaterial using a variety of methods including circular dichroism spectropolarimetry (CD), sedimentation velocity (SV), dynamic light scattering (DLS), and atomic force microscopy (AFM).[27] We found that, in the presence of crowding agents or high salt concentrations, polymerization could be induced that had the correct secondary structure and other morphological characteristics consistent with the design, and the polymers contained 10^2−10^3 peptides.

The motivation for the fundamental protein assembly work described in this article is rooted in our desire to gain a deeper

Received: July 6, 2011
Revised: September 1, 2011
Published: September 1, 2011

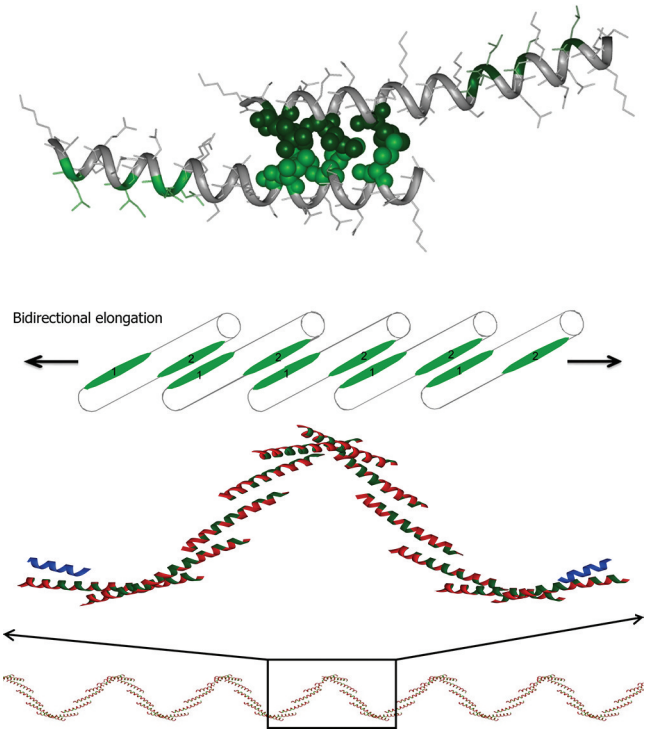

Figure 1. Structure schematics. Top figure: molecular model of offset interactions between a pair of helices. Side chains that are involved in hydrophobic interactions in GCN4 are shown in CPK representation and colored green. The ribbon is also colored green where hydrophobic residues would act as templates for the binding of additional peptides. Second figure: cartoon suggesting how phasing of hydrophobics leads to bidirectional elongation. The green patches highlight the 200° shift in phasing that is introduced by the two-alanine insertion between the 14-residue coiled-coil modules. Third figure: model building of successive offset interactions reveals higher order supercoiling, with capping peptides illustrated (blue), which can act to limit degree of polymerization. Bottom figure: predicted mesoscale structure of peptide polymers (these figures are reproduced or adapted from ref 27). Peptides used in this study:

```
                    1         2         3
          123456789012345678901234567890
                    abcdefgabcdefg  abcdefgabcdefg
CpA:      Ac-CKQLEDKIEELLSKAACKQLEDKIEELLSK-CONH2
CpA-I:    Ac-IKQLEDKIEELLSKAAIKQLEDKIEELLSK-CONH2
CpA-A:    Ac-AKQLEDKIEELLSKAAAKQLEDKIEELLSK-CONH2
CpA-N:    Ac-NKQLEDKIEELLSKAANKQLEDKIEELLSK-CONH2
CpA-S:    Ac-SKQLEDKIEELLSKAASKQLEDKIEELLSK-CONH2
CpA-S2:   Ac-IKQLEDKSEELLSKAAIKQLEDKSEELLSK-CONH2
```

understanding of the sequence−structure rules that govern larger scale coiled-coil assemblages, as described in that earlier work.[27] Specifically, we wanted to understand the importance of residues at the interfacial positions (by convention, the *a* and *d* heptad positions) in controlling the precise self-assembly of the coiled-coil polymers. We were interested in exploring how hydrophobic residues at these heptad positions influence both the stability and the degree of polymerization of these polymers. Others have also noted the importance of amino acid composition at the buried *a* and *d* heptad positions of coiled-coil designs on polymer assembly. Notably, Woolfson has applied proline-scanning mutagenesis at *d* positions to dissect the assembly path of their SAF system and has gained insight into the kinetics of axial and lateral assembly processes.[18] Conticello's laboratory has also mutated *d* positions, to introduce histidines at the helical interfaces of their coiled-coil polymers, and thus introduced a novel pH responsiveness to polymer assembly.[20]

An added advantage of our model system was that the resultant polymers remain in solution, thus allowing for a thermodynamic approach to studying their behavior using a noncovalent nucleation−elongation scheme.[28,29] There is a paucity of published papers applying a thermodynamic approach to the study of protein polymerization processes[30−33] since, more often than not, most protein polymers are simply too large to stay in solution.

We decided to focus on mutations at the *a* heptad position since greater tolerance for side chain identity is allowed. We varied the residues at two *a* heptad positions using isoleucine (CpA-I), alanine (CpA-A), asparagine (CpA-N), and serine (CpA-S) as our test residues (all sequences of the peptides used in this study are shown in the legend to Figure 1). This series allows us, in principle, to study how the stability and degree of polymerization of the coiled-coil polymers depend on hydrophobicity. Isoleucine was chosen because it is known to specify the dimeric coiled-coil oligomeric state.[23] Alanine and serine, containing small side chains, would not impose steric constraints on coiled-coil formation and would thus report more reliably on the importance of the hydrophobic effect on polymer characteristics. Finally, asparagine was of unique interest to us since it is known to impart structural specificity through pairwise H-bonding interactions at *a* heptad positions, albeit at the expense of coiled-coil stability.[24] Also, a thorough thermodynamic study of the effects of all 20 amino acids on coiled-coil stability at this heptad position has been carried out[34,35] and allowed us to compare our results to that determined for canonical coiled-coil model systems. Using these criteria to justify our approach, we characterized a set of peptides containing these mutations using a combined biophysical/thermodynamic approach.

MATERIALS AND METHODS

Peptide Synthesis and Purification. All peptides were purchased in crude form from AnaSpec (Fremont, CA) and were acetylated at the N-terminus and amidated at the C-terminus. Peptides were purified by RP-HPLC using a Varian ProStar system (Palo Alto, CA) equipped with a Varian Dynamax semipreparative C18 column. The mobile phase consisted of water and acetonitrile containing 0.1% TFA. Peptides were lyophilized and stored in a desiccator at −20 °C for long-term storage. Identities of products were verified by MALDI-TOF mass spectroscopy. Peptides were dissolved in water for storage in solution, and concentrations were determined by a modified ninhydrin procedure.[36]

Circular Dichroism Spectropolarimetry. Data were collected using an Aviv 62A circular dichroism spectropolarimeter. Measurements were made using a bandwidth of 1.5 nm. Thermal unfolding experiments were done using a 10 min equilibration time at each temperature step. All samples were prepared at 100 μM peptide concentration (unless otherwise noted) in 10 mM Tris-HCl, pH 8.0.

Analytical Ultracentrifugation. All data were collected using a Beckman ProteomeLab XL-A analytical ultracentrifuge equipped with an An60Ti rotor. For velocity experiments, standard two-sectored charcoal-filled Epon centerpieces and quartz windows were used with loading volumes of 435 μL for the peptide samples and 450 μL for the reference solution.

dx.doi.org/10.1021/bi201038j | *Biochemistry* 2011, 50, 8548−8558

Velocity experiments were run at a speed of 50 000 rpm and 25 °C. The partial specific volume, viscosity, and density parameters were calculated using SednTerp.[37] The data were analyzed using DCDT+ (v. 2.0.9, John Philo, Thousand Oaks, CA). For equilibrium experiments, six-sectored centerpieces were used with loading volumes of 115 μL for the peptide samples and 120 μL for the reference solution. Equilibrium experiments were run at 5000 rpm for analysis of the largest species and 20 000 and 50 000 rpm for analysis of smaller species, all at a temperature of 25 °C. Data were truncated using WinReedit (v. 0.999, 1998) and analyzed using WinNonLin (v. 1.035 1997).[38]

Dynamic Light Scattering. Data were collected using a DynaPro-MS/X dynamic light scattering instrument (Wyatt Technology, Santa Barbara, CA) equipped with an 825 nm laser and set at 10% power. Temperature was controlled using a DynaPro temperature-controlled microsampler. Instrument operation, data collection, and analysis were managed using the Dynamics (v. 6.0) software interface. Each stock solution was filtered using 0.2 μm HT Tuffryn membrane filters (Pall Corp., Ann Arbor, MI). Measurements were made using microcell cuvettes to minimize sample volume. For each sample, a set of eight independent measurements was made, with each measurement consisting of 30 runs each. The raw data for these experiments are shown in Figure S1. Time-dependent fluctuations in the scattered light were analyzed using a second-order correlation function. All samples were run at 25 °C in 10 mM Tris-HCl, pH 8.0. Data were analyzed assuming a linear polysaccharide model (included in the Dynamics software), which most closely approximates the shape of the polymers as determined in our earlier work.

Data Analysis Using Nucleation/Elongation Theory. Aggregation in solution can be modeled as a chemical equilibrium between monomers and polymers. An isodesmic model assumes an identical change in free energy for forming a nucleus vs extension of the nucleus, while a nucleation−elongation model assumes that the equilibrium constant for nucleus assembly differs from subsequent elongation steps. Our DLS and CD data are modeled with a nucleation−elongation model where we assume that the nucleus is a dimer and that dimerization is disfavored relative to chain growth. Specifically, we use the nucleation−elongation model as described by Zhao and Moore.[29]

Within this model, CD data were analyzed using eq 29 in ref 29:

$$C_t = (1 - \sigma)[A] + \frac{\sigma[A]}{(1 - K[A])^2} \quad (1)$$

which gives the total concentration on a per monomer basis, C_t, in terms of the final monomer concentration, [A], and parameters K (the elongation association constant) and a "nucleation factor" σ (the ratio of the dimerization association constant to K). Algebraic rearrangement yields an equation relating the surviving fraction of monomer $y = [A]/C_t$ to the scaled concentration $x = K \times C_t$. We assume that y is equal to the normalized CD mean residue ellipticity $[\theta]$, i.e., $y = ([\theta]_{exp} - [\theta]_{max})/([\theta]_{min} - [\theta]_{max})$, introducing two additional parameters $[\theta]_{min}$ (the CD signal corresponding to the monomer) and $[\theta]_{max}$ (the signal corresponding to the polymer). Given a set of CD data (C_t, $[\theta]$), we use the FindMinimum command in Mathematica (Version 8.0) to perform a nonlinear least-squares fit to this model, yielding best-fit values for K, σ, $[\theta]_{min}$, and $[\theta]_{max}$. Since the equation relating y to x cannot be solved explicitly for y, we find y numerically by Brent's method using Mathematica's FindRoot command (with some care taken in order for Brent's method to converge for very small or very large C_t). To improve the reliability of the numerics, we used $K_e = 1/K$ and $\log(\sigma)$ as parameters in place of K and σ. Sensitivity of the fit with respect to a parameter was assessed by varying the parameter slowly from its best-fit value, performing a least-squares fit over all other parameters, and assessing the change in quality of fit both visually and by the numerical change in the square root of variance.

As for the DLS data, we used eq 31 from ref 29 for the weight-averaged degree of polymerization:

$$\langle dp \rangle_w = \frac{\sigma(1 + K[A]) + (1 - \sigma)(1 - K[A])^3}{\sigma(1 - K[A]) + (1 - \sigma)(1 - K[A])^3} \quad (2)$$

Since eq 1 allows us to find $K[A]$ in terms of KC_t (again numerically via Brent's method), eq 2 can be reinterpreted to relate the DLS output $\langle dp \rangle_w$ to the concentration C_t and the model parameters K and σ. This relationship was used for least-squares fits of K and σ from DLS data (C_t, $\langle dp \rangle_w$), again using FindMinimum in Mathematica 8.0.

Atomic Force Microscopy. A 450 μM CpA-I sample in 10 mM Tris-HCl, pH 8.0, 0.3 M NaCl was incubated over a period of 48 h at 25 °C, deposited on freshly cleaved mica (SPI Supplies, West Chester, PA), and after 10 min the mica surface was washed using Milli-Q water and dried using high-quality N_2. Samples were imaged in tapping mode using a Bioscope atomic force microscope (Digital Instruments, Santa Barbara, CA). Data were analyzed using SigmaScan Pro (v. 5.0; SSI, San Jose, CA).

RESULTS

The sequences for the peptides used in this study are given in Figure 1 and are derived from our earlier work, in which we described the initial characterization of our coiled-coil polymer model system.[27] To explore the importance of the coiled-coil structure on polymerization, we made changes at positions 1 and 17, which represent the first and third *a* heptad core positions. We studied the effects of isoleucine (CpA-I), alanine (CpA-A), asparagine (CpA-N), and serine (CpA-S) on polymer assembly, all residues that are known to be tolerated at this core position in other coiled-coil model systems, with the expectation that a correlation between polymerization and hydrophobicity would be observed.

Since we expected an overlap of only 14 residues in the pairwise helical interactions (Figure 1), typical aqueous conditions would not suffice to drive coiled-coil formation. We had observed in our earlier work that salts drive coiled-coil assembly through their well-known salting-out effects. We first looked at the NaCl dependence of helix content using circular dichroism as a probe of structure (Figure 2). We note that the helix content develops fully within the time frame of sample preparation, and no changes in signal intensity are observed over a period of many hours in our CD experiments, suggesting no apparent kinetic effects. The estimated maximal theoretical molar ellipticity for a 30-amino-acid analogue, as measured at 222 nm and 25 °C, is −37 600 deg cm^2 dmol^{-1}.[39] CD spectra of 100 μM peptide show that CpA-I is almost 50% helical in the absence of salt, while for the other peptides, helicity is only around 17%. Sedimentation equilibrium studies confirm that all but CpA-I is monomeric in the absence of salt (CpA-I is 80%

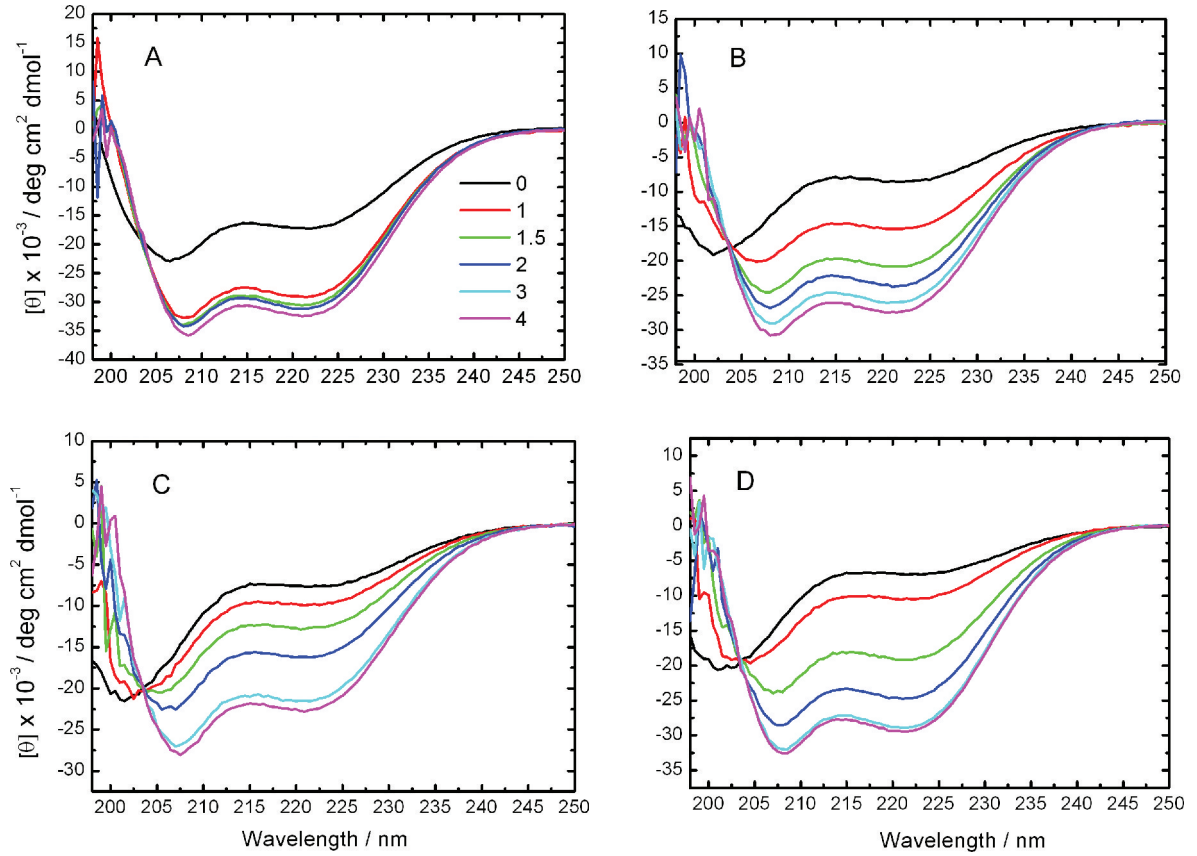

Figure 2. CD spectra as a function of NaCl for the peptides used in this study: (A) CpA-I, (B) CpA-A, (C) CpA-N, and (D) CpA-S. Peptides were all prepared at 100 μM each in 10 mM Tris-HCl, pH 8.0.

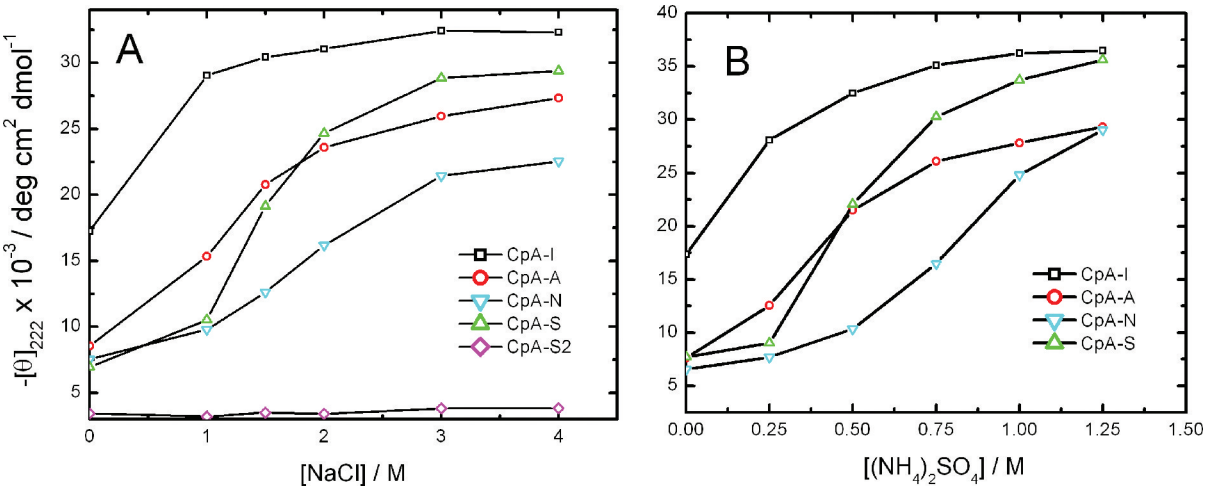

Figure 3. Dependence of CD signal, as monitored at 222 nm, as a function of (A) NaCl and (B) $(NH_4)_2SO_4$ for CpA-I, CpA-A, CpA-N, and CpA-S. Peptides were prepared at 100 μM each in 10 mM Tris-HCl, pH 8.0.

monomer by weight with the remainder consisting of polydisperse polymers). Thus, introducing a large hydrophobic group at these core positions appears to have a strong stabilizing effect on their resultant helical structure. We explored this in more detail by plotting the signal at 222 nm as a function of salt concentration for each of our peptides.

As noted previously,[27] the parent peptide, CpA, acquired helix content upon increasing NaCl concentration in a sigmoidal response as expected of a cooperative folding and assembly process. Maximal helix content was observed at about 4 M NaCl, and the mean residue ellipticity was consistent with a fully helical conformation. Placing an isoleucine at these *a* heptad positions (CpA-I) resulted in a very significant increase in helical stability since much less salt is needed to reach maximal helix content (Figure 3A). Surprisingly, CpA (not shown), CpA-A, and CpA-S show similar NaCl dependences with midpoints in their helical transitions in the range of 1.0−1.5 M NaCl, suggesting similar stabilities (Figure 3A and Table S1). CpA-N shows lower stability than any of the other peptides since the midpoint of the transition is at about 1.8 M

dx.doi.org/10.1021/bi201038j | *Biochemistry* 2011, 50, 8548−8558

NaCl and is significantly less helical at high salt than the other peptides in this study. Sedimentation equilibrium analysis of this peptide in high salt revealed an average molecular mass of 5000 ± 300 Da. We concluded that CpA-N did not form polymers, so no further experiments were performed on this peptide. Similar salt effects on all four peptides are observed when using $(NH_4)_2SO_4$, except that less salt is required to acquire the helical structure, consistent with the known impact of these salts on the strength of the hydrophobic effect (Figure S2, Figure 3B, and Table S1).

One explanation for why changes in residue polarity might not have the effects that we anticipated in our studies of CpA, CpA-A, and CpA-S is that these residues might be significantly solvated upon polymerization. This is certainly possible since the *a* heptad positions under consideration lie at the amino terminal end of each coiled-coil module. To test this hypothesis, we also synthesized a peptide (CpA-S2; sequence is given in Figure 1) in which the polar serine residues were moved to *a* heptad positions more centrally located within each coiled-coil module (positions 8 and 24) and thus are much more likely to be significantly desolvated upon folding and assembly. This peptide was unable to acquire helical structure upon addition of NaCl, suggesting that in such a weakly self-associating system, the salting-out effect is simply not sufficient to overcome the introduction of a polar residue in such a buried position (Figure 3A). Nevertheless, this peptide has the propensity to become helical since the addition of TFE resulted in a CD spectrum for that of a fully helical peptide (Figure S3). All further work in this article thus focuses on mutations only in the *a* heptad positions near the amino termini of each coiled-coil module (positions 1 and 17).

To further explore the cooperativity of folding and polymer assembly, we looked at the thermal unfolding behavior of CpA-I, again as measured by circular dichroism (Figure 4). We found

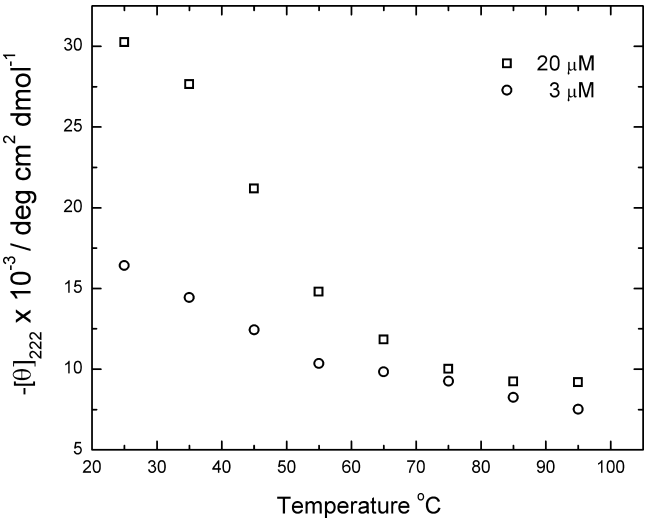

Figure 4. Thermal denaturation of CpA-I as monitored at CD at 222 nm. The sample was prepared in 10 mM Tris-HCl, pH 8.0.

that the peptide showed typical unfolding behavior as a function of temperature, indicating fairly high stability and a cooperative unfolding transition. The folding/unfolding transition was fully reversible (data not shown). More importantly, we saw a strong peptide concentration dependence to the polymer's thermal stability, indicating that the helical structure depends on higher order self-assembly. We initially explored the degree of polymerization of the four peptides using analytical ultracentrifugation.

Sedimentation velocity experiments were performed on each of the four peptides in the presence of 1.5 M NaCl to assess their degree of polymerization. However, due to artifacts on sedimentation imposed by the high concentration of salts required to promote self-assembly, we could not reach quantitative conclusions about polymer length or heterogeneity. Sedimentation velocity analysis revealed polydisperse polymers for all peptides but CpA-N with $s_{20,w}$ values in the range 6.0−6.2 Sv (Table 1). CpA-N did not sediment

Table 1. Sedimentation Velocity Behavior of CpA-X Peptides

peptides[a]	1.5 M NaCl	0.75 M $(NH_4)_2SO_4$
CpA	6.1[b]	5.0[b]
CpA-I	6.2	5.8
CpA-A	6.1	5.1
CpA-S	6.0	5.3
CpA-N	*c*	*c*

[a]All peptides were prepared at 100 μM concentration in the appropriate salt and 10 mM Tris-HCl, pH 8.0, and run in the ultracentrifuge at 25 °C. [b]Numbers reported are standardized $s_{20,w}$ values in units of svedbergs. [c]CpA-N sediments as a monomer.

appreciably, confirming the finding from our SE experiment (reported above). We also ran sedimentation velocity experiments in 0.75 M $(NH_4)_2SO_4$ and noted similar sedimentation behavior relative to that seen in NaCl (Table 1). These results are consistent with the results that we had previously published for CpA.[27]

We turned to a sedimentation equilibrium approach to more quantitatively address the degree of polymerization. We wanted to know if the degree of polymerization varied as a function of increasing salt concentration under conditions when the helical conformation was largely populated. To test this, we looked at the NaCl and $(NH_4)_2SO_4$ dependences of our most stable peptide, CpA-I (Table 2). Owing to the large size of the

Table 2. Sedimentation Equilibrium Behavior of CpA-I as a Function of Salt

[salt][a]	molecular mass (kDa)[b]
[NaCl]	
0.15 M	1900
0.30 M	1800
0.50 M	1600
0.75 M	2100
1.5 M	1600
[$(NH_4)_2SO_4$]	
0.15 M	1800
0.30 M	1800
0.5 M	1500

[a]All peptides were prepared at 100 μM concentration in the appropriate salt and 10 mM Tris-HCl, pH 8.0, and run in the ultracentrifuge at 25 °C. [b]Molecular masses are reported from fits to data collected at 5000 rpm.

polymers, we ran the analytical ultracentrifuge at the lowest speeds to most accurately reflect the average molecular masses of the polydisperse polymers. In the range 0.15−1.5 M NaCl,

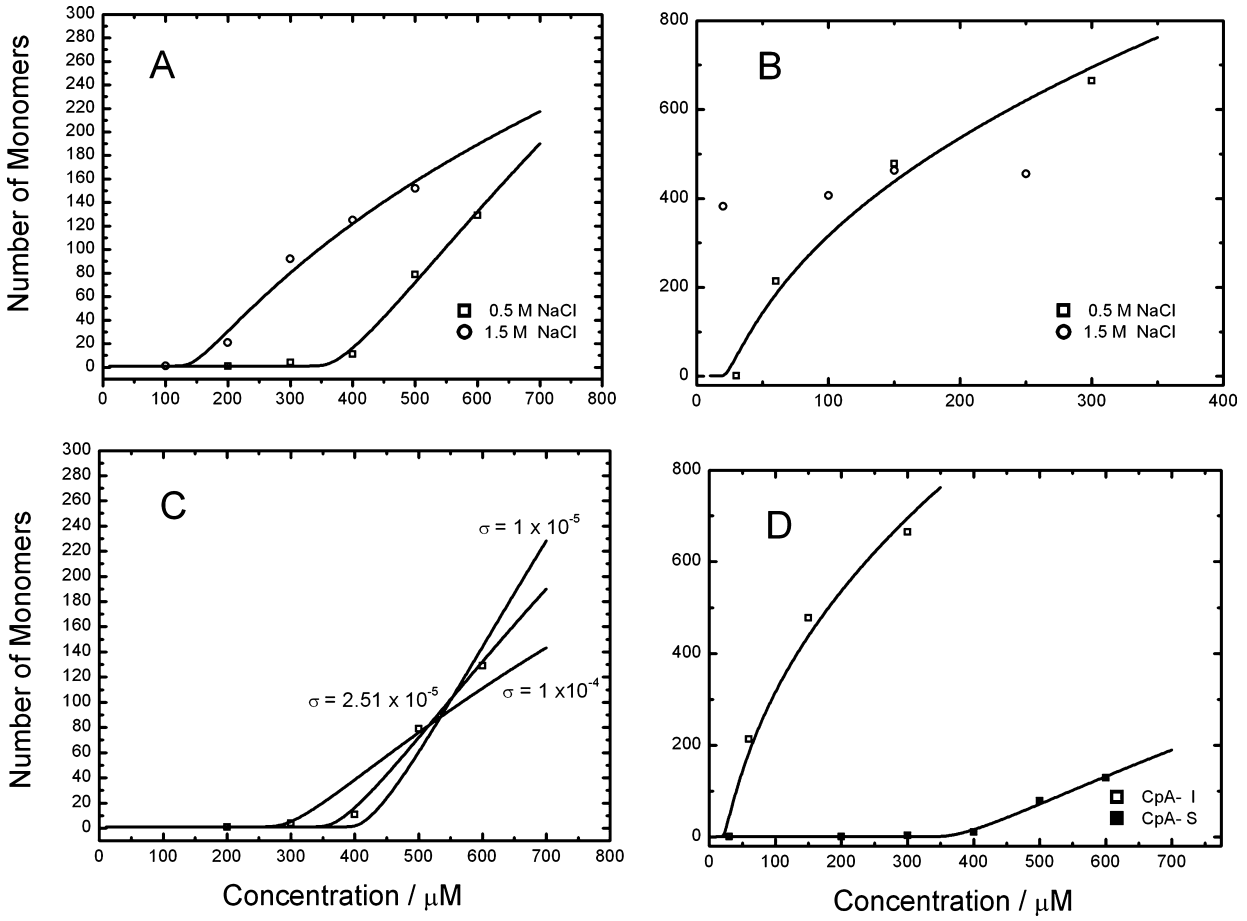

Figure 5. Polymer length as a function of peptide concentration as monitored by DLS for (A) CpA-S and (B) CpA-I. (C) CpA-S data collected in 0.5 M NaCl are shown with best-fit model ($\sigma = 2.5 \times 10^{-5}$) and models of $\sigma = 1 \times 10^{-4}$ and 1×10^{-5}. (D) Comparison of CpA-S and CpA-I in 0.5 M NaCl. Samples were prepared in 10 mM Tris-HCl, pH 8.0, and measured at 25 °C. All data (except for CpA-I in 1.5 M NaCl) are fit to eq 2 (Materials and Methods) to extract best-fit nucleation and elongation parameters. These parameters are presented in Table 3.

we observed little difference in the degree of polymerization, with average molecular masses ranging from 1600 to 2100 kDa. Although the CD results for CpA-I suggest incomplete polymerization in 0.15 M NaCl, the SE data are largely insensitive to monomer at the speed at which these experiments were run. Nevertheless, regardless of the fraction of peptide in the polymeric state, the data suggest that any polymer that forms is largely uniform in size with increasing NaCl concentration. A similar effect is observed as a function of $(NH_4)_2SO_4$ with a polymer mass range of 1500−1800 kDa. The lack of dependence of polymer length on salt concentration suggests that the induced hydrophobic effect is largely equal in energetics for both nucleation and elongation steps. We explored this question more quantitatively by applying the appropriate polymer nucleation−elongation theory to data collected by DLS and CD techniques.

We used DLS to look at the dependence of the degree of polymerization on peptide concentration, using CpA-S and CpA-I as our test systems (Figure 5). We collected data using either 0.5 or 1.5 M NaCl for both test peptides. CpA-S, being much less stable than CpA-I, requires significantly higher peptide concentrations to self-assemble into polymers (Figure 5A). As expected, at these same NaCl concentrations, CpA-I forms polymers at significantly lower peptide concentrations. For both peptides, the degree of polymerization did not change significantly when comparing 0.5 and 1.5 M NaCl (Figure 5B), consistent with our SE results.

The similar behavior of our polymers as studied by both DLS and SE suggests confidence in the fidelity of these two methods. This encouraged us to treat the DLS data reported in Figure 5 to a quantitative analysis to elucidate nucleation and elongation energetics. The data were fit to eq 2 as described in Materials and Methods, and the fits are shown in Figure 5. For curve-fitting purposes, we did not fit for the nucleation equilibrium constant directly; rather, we use the ratio of the nucleation association constant and the elongation association constant as a fitting parameter. Overall, the fits are quite robust, providing reasonable estimates of K_e (the dissociation constant governing elongation) and σ (the ratio of the nucleation and elongation equilibrium constants) for each condition. We could not fit the DLS data for CpA-I in 1.5 M NaCl since there is no increase in size with increasing peptide concentration. The parameters from the fits (K_e and σ) are shown in Table 3.

We focus first on an analysis of CpA-S (Figure 5A). The elongation dissociation constants for CpA-S are relatively large, indicating a weakly polymerizing system. The dissociation constant gets moderately smaller at higher NaCl concentration, suggesting that increasing NaCl enhances self-assembly, consistent with our CD data. The penalty for nucleation is very large for this peptide relative to its elongation, as reported by the very small values of σ (Table 3). This penalty,

dx.doi.org/10.1021/bi201038j | Biochemistry 2011, 50, 8548−8558

Table 3. Parameters Derived from Fitting of DLS and CD Data to a Nucleation–Elongation Mechanism

peptide (condition)	K_e[a]	σ[b]	ΔG_σ[c]	$[\theta]_{min}$[d]	$[\theta]_{max}$[d]
DLS experiments					
CpA-S (0.5 M NaCl)	3.6×10^{-4}	2.5×10^{-5}	6300		
CpA-S (1.5 M NaCl)	1.4×10^{-4}	2.2×10^{-4}	5000		
CpA-I (0.5 M NaCl)	2.1×10^{-5}	1.0×10^{-4}	5400		
CD experiments					
CpA-S (0.5 M NaCl)	1.7×10^{-4}	8.5×10^{-3}	2800	−7100	−37100
CpA-S (1.5 M NaCl)	7.7×10^{-5}	3.0×10^{-2}	2100	−7700	−36300
CpA-I (0.5 M NaCl)	2.1×10^{-5}	1.0×10^{-2}	2700	−12400	−41600
CpA-I (1.5 M NaCl)	9.2×10^{-6}	2.6×10^{-2}	2200	−12500	−44000

[a]Elongation dissociation constant reported in units of M. [b]Ratio of nucleation association constant and elongation association constant. [c]Free energy of σ reported in units of cal/mol. [d]CD parameters representing the monomer signal ($[\theta]_{min}$) and polymer signal ($[\theta]_{max}$) reported in units of deg cm^2 dmol^{-1}.

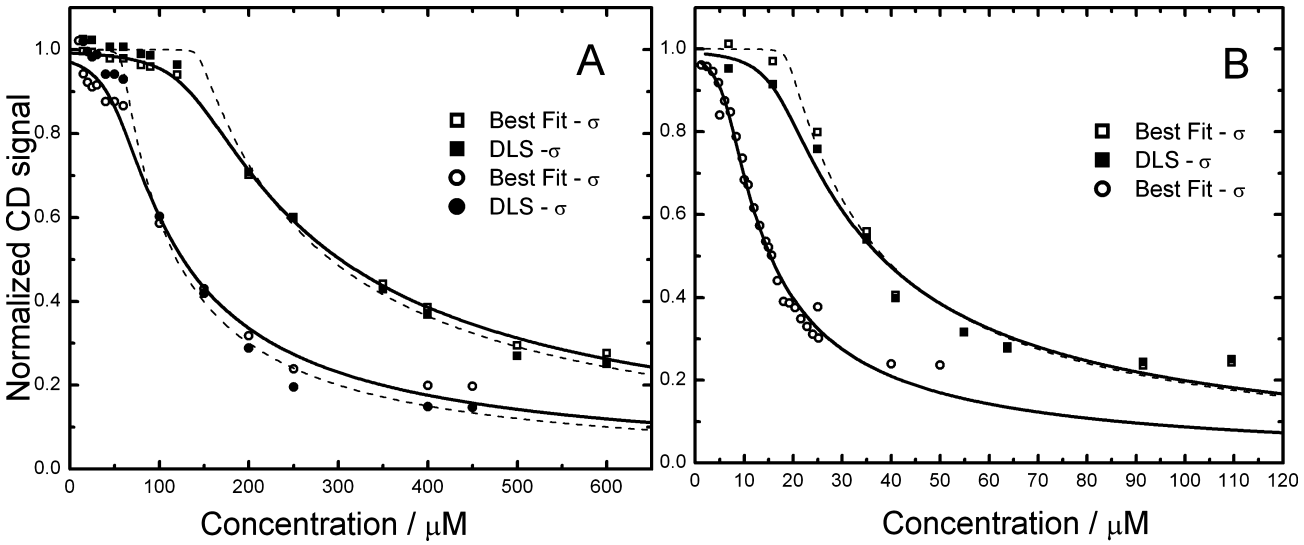

Figure 6. Normalized helix content (as measured by CD at 222 nm) as a function of peptide concentration for (A) CpA-S: squares represent 0.5 M NaCl data, and circles represent 1.5 M NaCl data; and (B) CpA-I: squares represent 0.5 M NaCl data, and circles represent 1.5 M NaCl data. Samples were prepared in 10 mM Tris-HCl, pH 8.0, and measured at 25 °C. The data are shown fit with eq 1 (Materials and Methods) to extract best-fit nucleation and elongation parameters. The normalized CD signal is determined by calculation of the fraction of helix content based on the best fit values of $[\theta]_{min}$ and $[\theta]_{max}$. As a consequence, for each separate curve fit, the data may be normalized to different values on the scale of zero to one; these different values are represented in the figures as closed or open symbols. Best Fit-σ refers to σ being treated as a fitting parameter, and this fit is represented with a solid line. DLS-σ refers to σ being fixed at the value determined from fitting of the DLS data as taken from Table 3, and this fit is represented with a dashed line. The parameters from the fits here are given in Table 3.

corresponding to positive free energies of ~6000 cal/mol, seems surprisingly large, if we were to assume that the dimeric nucleus is composed of the energy associated with a helical pairing interaction involving only 14-residue coiled-coil modules. This is discussed in greater detail below. There appears to be only a moderate impact of increasing NaCl on the value of σ for either peptide.

It should be pointed out that, in spite of the paucity of data points, the K_e and σ parameters are well determined. The value of K_e is very sensitive to the position of the midpoint in the peptide concentration isotherm, so even small changes in this parameter result in significant departures from good fits to the data. Furthermore, σ is also well determined. Figure 5C shows the same 0.5 M NaCl data for CpA-S with the original best-fit curve from Figure 5A compared to models in which the data are refit using fixed σ values deviating less than a log unit to either side from its best-fit value.

The parameter values derived from the fit of the CpA-I data collected in 0.5 M NaCl confirmed the qualitative results observed in the CD experiments described above in that this peptide forms polymers more readily than the other peptides in this study, indicating a modest but significant difference in the elongation energies (Figure 5B and Table 3). The σ parameters for CpA-I and CpA-S are similar when determined at the same salt concentration, and these results are discussed more fully in terms of the implications for our model in the Discussion section.

We also looked at the helix content (as measured at 222 nm) as a function of peptide concentration dependence for CpA-I and CpA-S in both 0.5 and 1.5 M NaCl (Figure 6). This technical approach focuses on partitioning the species between monomer and polymer rather than on determining the degree of polymerization and provides an independent method for analysis of fits using a nucleation–elongation scheme. The peptide concentration isotherms show the typical profiles for a polymerizing system, namely a sharp break in the signal as a function of increasing peptide concentration, which represents the critical concentration of monomer required for polymerization to occur. This break in the isotherm is followed by a gradual increase in the fraction of total peptide that is involved

dx.doi.org/10.1021/bi201038j | Biochemistry 2011, 50, 8548–8558

in the polymer. We fit these data to a nucleation−elongation mechanism, as described in eq 1 in the Materials and Methods. How sharp the initial break is depends upon the magnitude of σ. This parameter becomes ill determined in this type of experiment when the value of σ is quite small ($<10^{-3}$).[29] As a consequence, we were not able to extract these values with a high degree of confidence; in contrast, fitting of the elongation dissociation constants was more robust. In addition to the K_e and σ parameters, parameters for the helix contents of the peptide monomer, $[\theta]_{min}$, and polymer, $[\theta]_{max}$, are also included as fitting parameters. The requirement of fitting these additional values adds to greater uncertainty in the best-fit values of K_e and σ.

We report the parameters from fitting of the CpA-S data presented in Figure 6A in Table 3. The elongation dissociation constants in 0.5 and 1.5 M NaCl are significantly smaller than those reported in the DLS experiments. Fits to the data fixing K_e to the values reported from DLS result in a significant increase in the square root of variance of the fit to the data, suggesting a poorer fit. We also note a dramatic increase in the best-fit value for the σ parameter when comparing the fits to the CD data with the fits to the DLS data. However, as noted above, the quality of the fits to the data appears to be relatively insensitive to changes in this parameter. Fits to the CD data using the best-fit σ values from the DLS data (Figure 6A) are not very different at high peptide concentrations (where the polymerization process is dominated by elongation) and only marginally different at lower peptide concentrations, as judged by differences in the square roots of variance for the two models. In anticipating this problem, we aimed to collect more data at the point where the initial break in the curve occurs, and upon visual inspection, we note that there is an improved fit to the data at this breakpoint when σ is allowed to vary. The σ parameter, when kept fixed at the value determined from DLS experiments, predicts a significantly steeper break.

The differences in the K_e and σ values as determined by using DLS or CD experiments initially concerned us since one possibility is that one of the two methods was giving us artifactual results. However, on further reflection, we thought that the two techniques might be revealing greater complexity in the number of stable states involved in self-assembly. We hypothesized that the nucleation−elongation mechanism might involve the formation of a stable intermediate, an idea that we could test using an SE approach. On what basis do we infer the presence of an intermediate based on the DLS and CD analysis? The CD technique monitors acquisition of helix content, so whether a polymer is short (on the order of ten peptide units) or long, we would expect to see the same change in signal intensity at 222 nm. If a short, stable intermediate is formed, then the value of the nucleation parameter would be dominated by the transition state energy necessary to reach this intermediate. In contrast, short polymers would be largely transparent in the DLS experiments since even a small amount of large polymers would dominate the signal observed by this technique. Hence, if an intermediate were present, then the DLS would instead monitor the nucleation−elongation mechanism of the assembly of short polymer intermediates into the larger scale structures that are formed.

A careful reanalysis of the SE data collected for CpA-S at higher speeds was performed, in which the larger molecular mass species would be depleted from the window of observation, thus leaving us with an opportunity to detect monomeric and small oligomeric species. The goal was to compare fits to the CpA-S data at various peptide concentrations to either two species (monomer and large polymer) or three species (monomer, oligomer, and large polymer) models. We looked at concentrations of 200, 250, and 300 μM CpA-S where the DLS data showed relatively low amounts of large polymers while the CD data predicted high levels of helix content. The goodness of fit, as measured by the square root of variance, for two-species models for these three concentrations were 7.11, 8.51, and 5.95, respectively. Inclusion of a third state significantly improved the fits, resulting in square roots of variance of 6.06, 7.57, and 4.90 for these same concentrations. The molecular masses for this third state predicted an oligomeric state containing 15−30 peptides, which we assess as being in the size range that would influence the CD assay and would not be easily visible by DLS. It is important to point out that these polymers are unlikely to be homogeneous, rather that both oligomeric and polymeric species are likely to be polydisperse. While we fit the data to discrete states, we recognize this fitting approach is a simple approximation of the real situation.

We now turn to a brief quantitative analysis of the CD data for CpA-I. In contrast to the results with CpA-S, we note a smaller increase in σ in comparing the DLS and CD experiments for CpA-I in 0.5 M NaCl (Figure 6B and Table 3). As a point of comparison, we show a fit to these same data using the σ value determined from the DLS experiment. There is at most only a moderate decrease in the quality of the fit, revealing the insensitivity of the CD approach to significant variations in the value for σ, as noted above. It is possible that this smaller discrepancy between the DLS and CD analysis suggests a change in the population (or size) of the putative oligomeric intermediate, as compared to what we proposed for the CpA-S case. Interestingly, we see no difference in the values of K_e for CpA-I in 0.5 M NaCl when comparing the DLS and CD data.

Overall, we show quantitatively that increasing the contribution of the hydrophobic effect, either through mutation or through a salting-out effect, results in a significant increase in polymer stability, consistent with the coiled coil being a major feature of our model system. Interestingly though, we see no significant difference in the degree of polymerization for the mutation of a core isoleucine to the more polar serine or upon increasing salt.

Finally, we briefly describe representative images of the morphology of the CpA-I peptide using atomic force microscopy. The AFM images are shown in Figure 7 (prepared with NaCl) and Figure S4 (prepared with $(NH_4)_2SO_4$). Our goal was simply to compare these morphologies to what we had observed for CpA in our previously published work, and we found that there are no significant differences from our previously published work.[27] Overall, we saw longer filaments for CpA-I than we did with our parent peptide, CpA, but the widths, heights, and degree of polydispersity were quite similar. More detailed characterizations of the fibrillar morphologies for these peptides will be explored in future work.

DISCUSSION

We have applied a thermodynamic analysis of the polymerizing potential of our coiled-coil model system that we first described a number of years ago.[27] Our goal was to understand in more detail the role of the hydrophobic effect on polymer growth and stability with the hope that it would lead to an improved understanding of the design elements needed to create

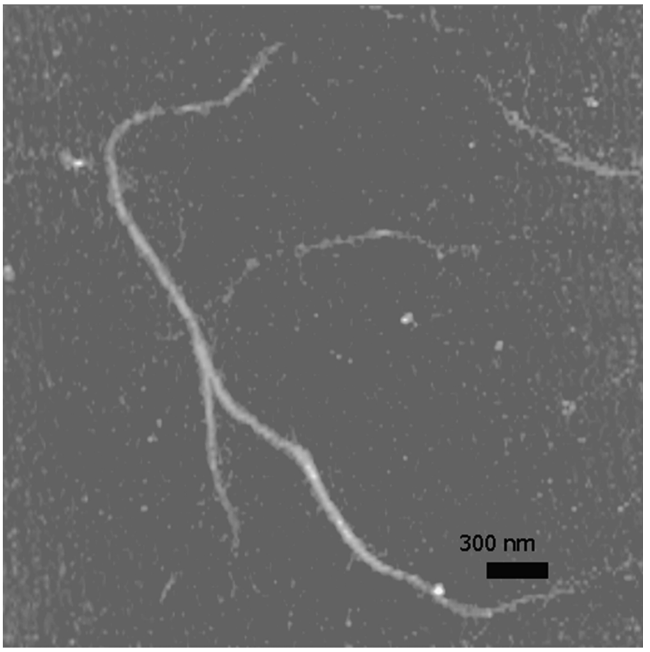

Figure 7. AFM image of 450 μM CpA-I in 0.3 M NaCl and 10 mM Tris-HCl, pH 8.0. The sample was prepared on a mica surface as described in Materials and Methods.

photoelectronic biomaterials. We have since used similar sequences to create photoelectronically active materials by incorporating porphyrins into the design.[40,41]

We first took a qualitative approach to test our model by analyzing the effects of mutations at core, *a* heptad, positions, in which we varied the degree of polarity of the residues. As expected, we found that isoleucine, the most hydrophobic residue in our series, offered the greatest stability. In comparison, mutations to alanine or serine resulted in significant destabilization, both approximately equal in their effects. The similar stabilities in CpA-A, CpA-S, and our parent peptide, CpA, suggest that the positions that we mutated are likely to be significantly solvent exposed, and this conclusion was supported by the greater destabilizing effects of serine mutations that were introduced more centrally in the coiled-coil modules. Asparagine completely abrogated polymer assembly for reasons that are not fully understood given their tolerance at *a* heptad positions in other coiled coils. These qualitative findings generally support the predictions of the secondary and tertiary structures from our model, as presented in Figure 1. As expected, salts, such as NaCl and $(NH_4)_2SO_4$, increase the propensity to form polymers, since such salts are known to enhance the hydrophobic effect.

These initial studies revealed stable polymers that remain in solution, allowing us to apply thermodynamic approaches to determine nucleation and elongation properties. Results from our CD data suggest that they sensitively probe smaller states (representing putative assembly intermediates) in polymer assembly, and we interpret the results in terms of a dimeric helix pairing interaction as the putative nucleus. We note first that there is little change in the value of σ upon mutation of isoleucine to serine when considering the CD data. The $\Delta\Delta G_\sigma$ for this mutation (calculated using the ΔGs reported for σ in Table 3) are −0.09 and 0.08 kcal/mol for the 0.5 and 1.5 M NaCl data, respectively. These results indicate that the mutation does not impact the relative nucleation and elongation energies for polymerization. A similar conclusion is reached when comparing the σ values as determined from the DLS data.

It is also useful to compare the $\Delta\Delta G$ of the isoleucine to serine mutation for the elongation step. On the basis of the elongation dissociation constants reported in Table 3 as determined from the CD data, we find that the $\Delta\Delta G$s for the 0.5 and 1.5 M NaCl data are 1.23 and 1.25 kcal/mol/monomer, respectively (the DLS data give a similar $\Delta\Delta G$ of 0.87 kca/mol/monomer). This $\Delta\Delta G$ can be compared to previous work from two other laboratories, which reported that such a mutation at the same heptad position using a canonical coiled-coil model system results in a free energy difference ranging from 4.5 to 5.5 kcal/mol/monomer.[34,35] The much smaller $\Delta\Delta G$ that we observe for this mutation most likely reflects the interpretation we had proposed above, namely that there is significant solvation of residues at this position, resulting in a damping of the hydrophobic contribution to stability upon only partial burial of the isoleucine. This conclusion is bolstered by the fact that a much larger impact on stability is observed when the mutation is made at the *a* heptad positions that are more centrally located in the coiled-coil module.

To complete the thermodynamic analysis, we can also compare changes in free energy upon increasing salt concentration. The $\Delta\Delta G$, again as calculated using the CD data, for σ is −0.74 kcal/mol (−1.30 kcal/mol using the DLS data) for CpA-S and −0.57 kcal/mol for CpA-I in going from 0.5 M NaCl to 1.5 M NaCl. We infer that this is related to the energetics of the salting-out effect; it is unwarranted to draw a conclusion about the difference in such an effect on burying a serine vs an isoleucine given the small differences in these free energies.

The thermodynamic analysis provided here, using a nucleation−elongation model, confirms and quantifies the conclusions that we had reached regarding the importance of the hydrophobic effect on the stabilities and degrees of polymerization in our coiled-coil model system. The analysis of our data further supports the model of assembly involving offset helical pairing interactions that we had proposed in our earlier work and has given us a more complex view of the number of states involved that likely contains at least two discrete assembly steps. Similar ideas for assembly have been recently proposed by the Woolfson laboratory.[18] We had originally argued that assembly proceeded via a step-growth polymerization model based on the ability to compete out the polymerization with a "capping" peptide (a peptide containing only one hydrophobic module).[27] This conclusion is not inconsistent with our present findings since step-growth mechanisms typically imply the size of the unit added on during elongation and do not necessarily distinguish between isodesmic and nucleation/elongation polymerization processes. Such findings will certainly illuminate our long-term goals of creating mesoscale photoelectronically active biomaterials from the ground up.

■ ASSOCIATED CONTENT

Ⓢ Supporting Information

DLS autocorrelation curves used to extract size information for analysis using nucleation/elongation theory (Figure S1), midpoints of the salt titration CD experiments (Table S1), CD spectra of the four peptides in this study as a function of increasing $(NH_4)_2SO_4$ (Figure S2), CD spectra of CpA-S2 in TFE or as a function of NaCl concentration (Figure S3), and atomic force microscope image of CpA-I in 0.75 M $(NH_4)_2SO_4$

(Figure S4). This material is available free of charge via the Internet at http://pubs.acs.org.

AUTHOR INFORMATION

Corresponding Author

*Tel: (610) 896-4205. Fax: (610) 896-4963. E-mail: rfairman@haverford.edu.

Funding

This research was supported by NSF grant MCB-0516025 to R.F. and a grant to Haverford College from the HHMI Undergraduate Science Education Program to support undergraduate research.

ACKNOWLEDGMENTS

We thank Dr. Walter Smith for training in the use of the AFM and Dr. William DeGrado for the use of his MALDI-TOF mass spectrometer. We also thank Cristina Fuller for editing the manuscript.

ABBREVIATIONS

AFM, atomic force microscopy; CD, circular dichroism spectropolarimetry; DLS, dynamic light scattering; MALDI-TOF, matrix-assisted laser desorption/ionization-time-of-flight; SE, sedimentation equilibrium; SV, sedimentation velocity.

REFERENCES

(1) Kyle, S., Aggeli, A., Ingham, E., and McPherson, M. J. (2009) Production of self-assembling biomaterials for tissue engineering. *Trends Biotechnol. 27*, 423−433.

(2) Chen, C. L., and Rosi, N. L. (2010) Peptide-Based Methods for the Preparation of Nanostructured Inorganic Materials. *Angew. Chem., Int. Ed. 49*, 1924−1942.

(3) McAllister, K. A., Zou, H., Cochran, F. V., Bender, G. M., Senes, A., Fry, H. C., Nanda, V., Keenan, P. A., Lear, J. D., Saven, J. G., Therien, M. J., Blasie, J. K., and DeGrado, W. F. (2008) Using alpha-helical coiled-coils to design nanostructured metalloporphyrin arrays. *J. Am. Chem. Soc. 130*, 11921−11927.

(4) Fairman, R., and Akerfeldt, K. S. (2005) Peptides as novel smart materials. *Curr. Opin. Struct. Biol. 15*, 453−463.

(5) Pepe-Mooney, B. J., and Fairman, R. (2009) Peptides as materials. *Curr. Opin. Struct. Biol. 19*, 483−494.

(6) Whitesides, G. M., Mathias, J. P., and Seto, C. T. (1991) Molecular self-assembly and nanochemistry: a chemical strategy for the synthesis of nanostructures. *Science 254*, 1312−1319.

(7) Chockalingam, K., Blenner, M., and Banta, S. (2007) Design and application of stimulus-responsive peptide systems. *Protein Eng., Des. Sel. 20*, 155−161.

(8) Krishna, O. D., and Kiick, K. L. (2010) Protein- and Peptide-Modified Synthetic Polymeric Biomaterials. *Biopolymers 94*, 32−48.

(9) Apostolovic, B., Danial, M., and Klok, H. A. (2010) Coiled coils: attractive protein folding motifs for the fabrication of self-assembled, responsive and bioactive materials. *Chem. Soc. Rev. 39*, 3541−3575.

(10) Woolfson, D.N. (2010) Building Fibrous Biomaterials From alpha-Helical and Collagen-Like Coiled-Coil Peptides. *Biopolymers 94*, 118−127.

(11) Woolfson, D. N., and Mahmoud, Z. N. (2010) More than just bare scaffolds: towards multi-component and decorated fibrous biomaterials. *Chem. Soc. Rev. 39*, 3464−3479.

(12) Gribbon, C., Channon, K. J., Zhang, W., Banwell, E. F., Bromley, E. H., Chaudhuri, J. B., Oreffo, R. O., and Woolfson, D. N. (2008) MagicWand: a single, designed peptide that assembles to stable, ordered alpha-helical fibers. *Biochemistry 47*, 10365−10371.

(13) Pandya, M. J., Spooner, G. M., Sunde, M., Thorpe, J. R., Rodger, A., and Woolfson, D. N. (2000) Sticky-end assembly of a designed peptide fiber provides insight into protein fibrillogenesis. *Biochemistry 39*, 8728−8734.

(14) Papapostolou, D., Brornley, E. H. C., Bano, C., and Woolfson, D. N. (2008) Electrostatic control of thickness and stiffness in a designed protein fiber. *J. Am. Chem. Soc. 130*, 5124−5130.

(15) Ryadnov, M. G., Ceyhan, B., Niemeyer, C. M., and Woolfson, D. N. (2003) "Belt and braces": a peptide-based linker system of de novo design. *J. Am. Chem. Soc. 125*, 9388−9394.

(16) Ryadnov, M. G., and Woolfson, D. N. (2003) Introducing branches into a self-assembling peptide fiber. *Angew. Chem., Int. Ed. 42*, 3021−3023.

(17) Ryadnov, M. G., and Woolfson, D. N. (2003) Engineering the morphology of a self-assembling protein fibre. *Nature Mater. 2*, 329−332.

(18) Bromley, E. H., Channon, K. J., King, P. J., Mahmoud, Z. N., Banwell, E. F., Butler, M. F., Crump, M. P., Dafforn, T. R., Hicks, M. R., Hirst, J. D., Rodger, A., and Woolfson, D. N. (2010) Assembly pathway of a designed alpha-helical protein fiber. *Biophys. J. 98*, 1668−1676.

(19) Dublin, S., Zimenkov, Y., and Conticello, V. P. (2009) Engineering responsive mechanisms to control the assembly of peptide-based nanostructures. *Biochem. Soc. Trans. 37*, 653−659.

(20) Dublin, S. N., and Conticello, V. P. (2008) Design of a selective metal ion switch for self-assembly of peptide-based fibrils. *J. Am. Chem. Soc. 130*, 49−51.

(21) Lu, K., Guo, L., Mehta, A. K., Childers, W. S., Dublin, S. N., Skanthakumar, S., Conticello, V. P., Thiyagarajan, P., Apkarian, R. P., and Lynn, D. G. (2007) Macroscale assembly of peptide nanotubes. *Chem. Commun. (Cambridge, U. K.)*, 2729−2731.

(22) Zimenkov, Y., Dublin, S. N., Ni, R., Tu, R. S., Breedveld, V., Apkarian, R. P., and Conticello, V. P. (2006) Rational design of a reversible pH-responsive switch for peptide self-assembly. *J. Am. Chem. Soc. 128*, 6770−6771.

(23) Harbury, P. B., Zhang, T., Kim, P. S., and Alber, T. (1993) A switch between two-, three-, and four-stranded coiled coils in GCN4 leucine zipper mutants. *Science 262*, 1401−1407.

(24) Lumb, K. J., and Kim, P. S. (1995) A buried polar interaction imparts structural uniqueness in a designed heterodimeric coiled coil. *Biochemistry 34*, 8642−8648.

(25) O'Shea, E. K., Klemm, J. D., Kim, P. S., and Alber, T. (1991) X-ray structure of the GCN4 leucine zipper, a two-stranded, parallel coiled coil. *Science 254*, 539−544.

(26) O'Shea, E. K., Rutkowski, R., and Kim, P. S. (1989) Evidence that the leucine zipper is a coiled coil. *Science 243*, 538−542.

(27) Wagner, D. E., Phillips, C. L., Ali, W. M., Nybakken, G. E., Crawford, E. D., Schwab, A. D., Smith, W. F., and Fairman, R. (2005) Toward the development of peptide nanofilaments and nanoropes as smart materials. *Proc. Natl. Acad. Sci. U. S. A. 102*, 12656−12661.

(28) Oosawa, F. (1970) Size distribution of protein polymers. *J. Theor. Biol. 27*, 69−86.

(29) Zhao, D. H., and Moore, J. S. (2003) Nucleation-elongation: a mechanism for cooperative supramolecular polymerization. *Org. Biomol. Chem. 1*, 3471−3491.

(30) Chirita, C. N., Congdon, E. E., Yin, H., and Kuret, J. (2005) Triggers of full-length tau aggregation: a role for partially folded intermediates. *Biochemistry 44*, 5862−5872.

(31) Congdon, E. E., Kim, S., Bonchak, J., Songrug, T., Matzavinos, A., and Kuret, J. (2008) Nucleation-dependent tau filament formation: the importance of dimerization and an estimation of elementary rate constants. *J. Biol. Chem. 283*, 13806−13816.

(32) de Greef, T. F., Ercolani, G., Ligthart, G. B., Meijer, E. W., and Sijbesma, R. P. (2008) Influence of selectivity on the supramolecular polymerization of AB-type polymers capable of Both A x A and A x B interactions. *J. Am. Chem. Soc. 130*, 13755−13764.

(33) Chang, E., Kim, S., Yin, H., Nagaraja, H. N., and Kuret, J. (2008) Pathogenic missense MAPT mutations differentially modulate tau aggregation propensity at nucleation and extension steps. *J. Neurochem. 107*, 1113−1123.

(34) Wagschal, K., Tripet, B., Lavigne, P., Mant, C., and Hodges, R. S. (1999) The role of position a in determining the stability and oligomerization state of alpha-helical coiled coils: 20 amino acid

stability coefficients in the hydrophobic core of proteins. *Protein Sci. 8*, 2312−2329.
(35) Acharya, A., Rishi, V., and Vinson, C. (2006) Stability of 100 homo and heterotypic coiled-coil a-a' pairs for ten amino acids (A, L, I, V, N, K, S, T, E, and R). *Biochemistry 45*, 11324−11332.
(36) Rosen, H. (1957) A modified ninhydrin colorimetric analysis for amino acids. *Arch. Biochem. Biophys. 67*, 10−15.
(37) Laue, T. M., Shah, B. D., Ridgeway, T. M., and Pelletier, S. L. (1992) Computer-Aided Interpretation of Analytical Sedimentation Data for Proteins, in *Analytical Ultracentrifugation in Biochemistry and Polymer Science* (Harding, S. E., Rowe, A. J., and Horton, J. C., Eds.) The Royal Society of Chemistry, Cambridge, UK.
(38) Johnson, M.L., Correia, J. J., Yphantis, D. A., and Halvorson, H. R. (1981) Analysis of data from the analytical ultracentrifuge by nonlinear least-squares techniques. *Biophys. J. 36*, 575−588.
(39) Rohl, C. A., and Baldwin, R. L. (1998) Deciphering rules of helix stability in peptides. *Methods Enzymol. 295*, 1−26.
(40) Kokona, B., Kim, A. M., Roden, R. C., Daniels, J. P., Pepe-Mooney, B. J., Kovaric, B. C., de Paula, J. C., Johnson, K. A., and Fairman, R. (2009) Self assembly of coiled-coil peptide-porphyrin complexes. *Biomacromolecules 10*, 1454−1459.
(41) Kovaric, B. C., Kokona, B., Schwab, A. D., Twomey, M. A., de Paula, J. C., and Fairman, R. (2006) Self-assembly of peptide porphyrin complexes: toward the development of smart biomaterials. *J. Am. Chem. Soc. 128*, 4166−4167.

SUPPORTING INFORMATION

Thermodynamic analysis of self-assembly in coiled-coil biomaterials.

Betty P. Tsang,[‡] Heidi S. Bretscher,[‡] Bashkim Kokona,[‡] Robert S. Manning,[§] and Robert Fairman[‡]*

[‡]Department of Biology, Haverford College, 370 Lancaster Ave, Haverford, PA 19041

[§]Department of Mathematics, Haverford College, 370 Lancaster Ave, Haverford, PA 19041

Table S1. Midpoints in salt dependence experiments as measured by CD.

Peptide	**[NaCl] (M)**	**[$(NH_4)_2SO_4$] (M)**
CpA	1.4	0.45
CpA-I	0.1	0.25
CpA-A	1.2	0.40
CpA-S	1.5	0.55
CpA-N	1.8	0.80

Figure S1. DLS autocorrelation data that were used for the data analysis presented Figure 5 and Table 3. (A) CpA-I in 0.5 M NaCl; (B) CpA-S in 0.5 M NaCl; (C) CpA-S in 1.5 M NaCl; (D) CpA-I in 1.5 M NaCl.

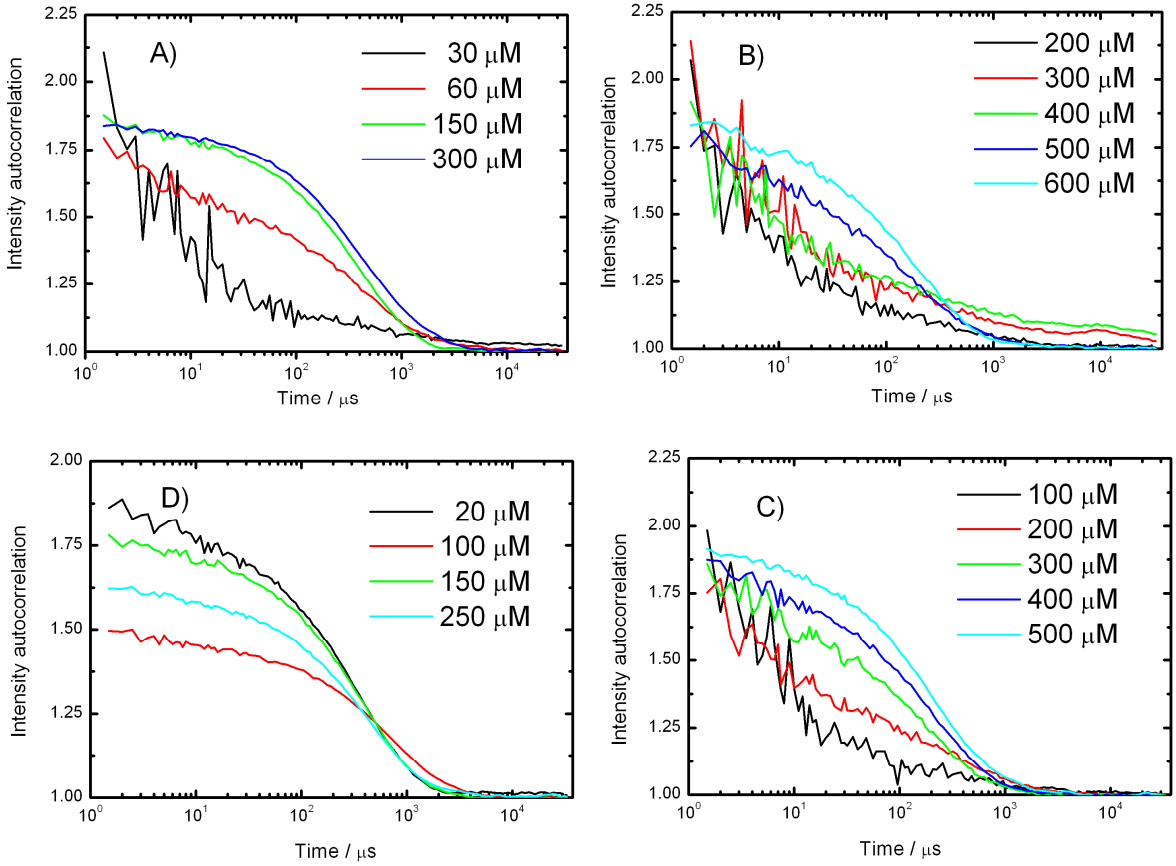

Figure S2. CD spectra as a function of $(NH_4)_2SO_4$ for the peptides used in this study. (A) CpA-I; (B) CpA-A; (C) CpA-N; (D) CpA-S. Peptides were prepared at 100 μM each in 10 mM Tris-HCl, pH 8.0.

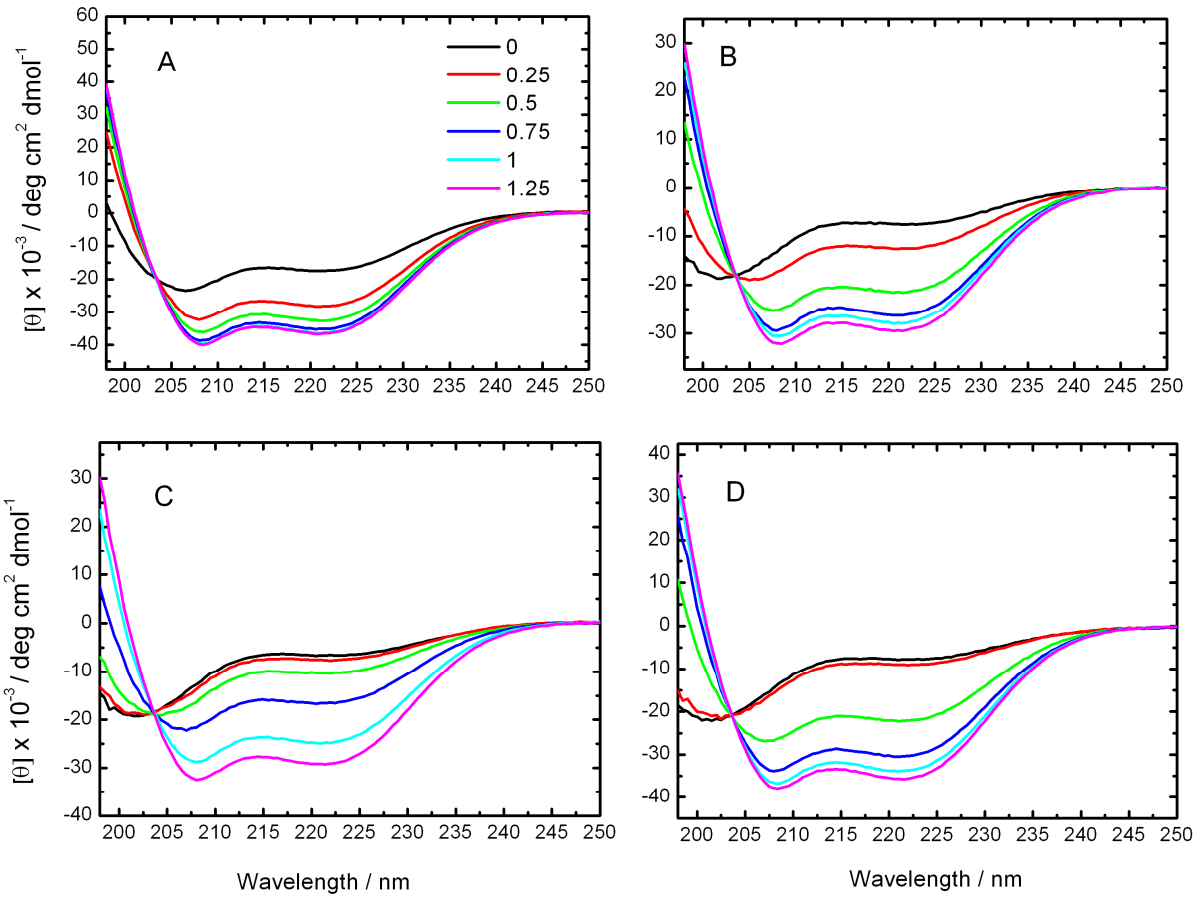

Figure S3. CD spectra of 100 μM CpA-S1 in trifluorethanol or various concentrations of NaCl.

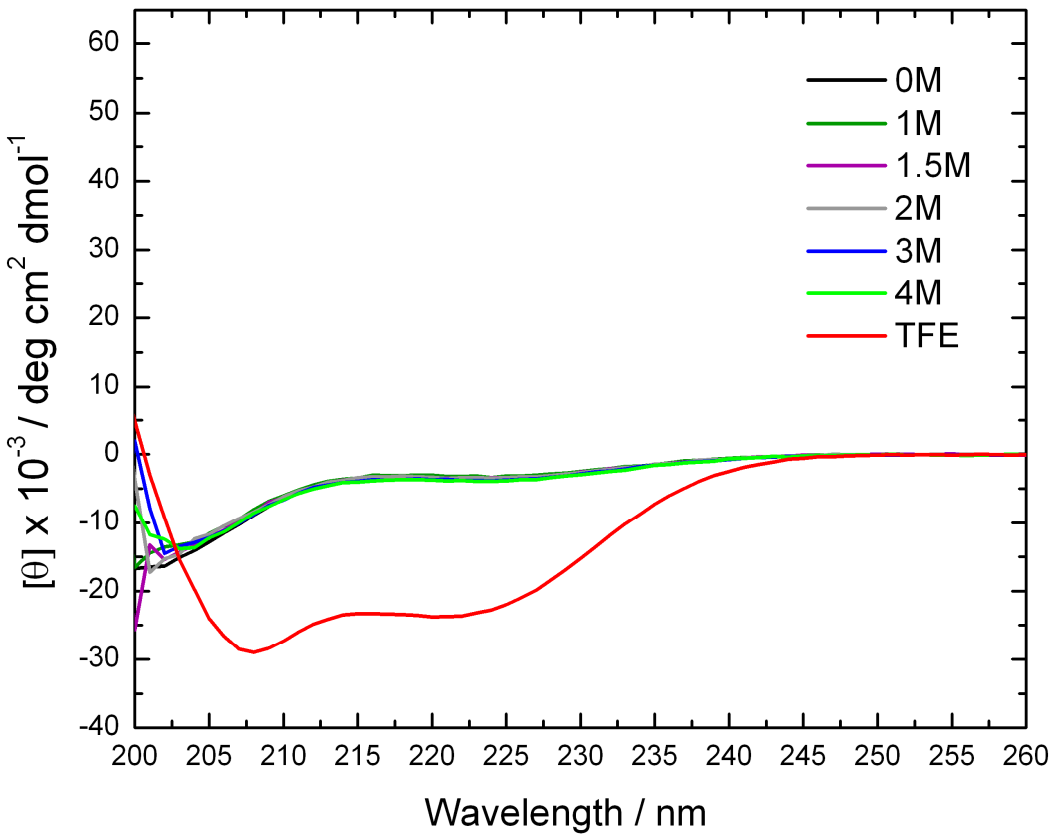

Figure S4. AFM image of CpA-I in the presence of 0.75 M $(NH_4)_2SO_4$ at the same peptide concentration and buffer conditions as reported in Figure 7. Sample preparation was slightly different as that reported in the Materials and Methods in that the sample was incubated at 4°C for a period of 7 hours prior deposition on mica.